Asian Journal of Pharmaceutical Sciences 21 (2026) 101122

Available online at www.sciencedirect.com

ScienceDirect

journal homepage: www.elsevier.com/locate/AJPS



Research Article

Inhalable stem cell-derived artificial nanovesicles for targeted siRNA delivery to effectively alleviate asthma symptoms

Shihan Chen[a,b], *Ruyi Lin*[a], *Yuhuan Kong*[a], *Hao Sun*[a], *Jiawen Wang*[a], *Jinsong Zhang*[a], *Yanshuang Huang*[a,c], *Honghui Wu*[a,c], *Donghang Xu*[d,*], *Jianqing Gao*[a,b,c,e,*], *Tianyuan Zhang*[a,b,e,*]

[a] *School of Pharmacy, Zhejiang University, Hangzhou 310058, China*
[b] *Hangzhou Institute of Innovative Medicine, School of Pharmacy, Zhejiang University, Hangzhou 310058, China*
[c] *Jinhua Institute of Zhejiang University, Jinhua 321000, China*
[d] *Department of Pharmacy, The Second Affiliated Hospital, Zhejiang University School of Medicine, Hangzhou 310009, China*
[e] *State Key Laboratory of Advanced Drug Delivery and Release Systems, Zhejiang University, Hangzhou 310058, China*

ARTICLE INFO

Article history:
Received 24 March 2025
Revised 10 October 2025
Accepted 12 November 2025
Available online 12 January 2026

Keywords:
Nanovesicles
Mesenchymal stem cells
Inhalation
siRNA delivery
Asthma

ABSTRACT

Asthma, one of the most prevalent chronic inflammatory diseases, remains challenging to manage effectively. Current therapies commonly alleviate symptoms through broad immunosuppression and bronchodilation but fail to target disease-specific molecular pathways. Genetic intervention using small interfering RNA (siRNA) has emerged as a promising strategy for asthma therapy. However, its success is largely hindered by the lack of an efficient delivery approach targeting airway epithelial cells (AECs). Here, we developed a novel inhalable siRNA delivery system based on artificially prepared nanovesicles through designed extrusion processes of mesenchymal stem cells. To enable an effective inhalation delivery of siRNA *via* nanovesicles, various parameters, including extrusion cycles, membrane pore sizes, and centrifugal forces were examined through orthogonal testing. Results revealed that the artificially prepared nanovesicles demonstrated remarkable capability to deliver thymic stromal lymphopoietin-targeted siRNA into AECs and substantially suppressed the inflammatory pathways and goblet cell hyperplasia, and eventually achieved a significant inhibition of asthma symptoms in ovalbumin-induced asthma models. Thus, the present study provides a novel nebulized nanovesicle-based carrier for effective delivery of siRNA through local inhalation, offering a promising therapeutic delivery platform for asthma and potentially other respiratory diseases.

© 2026 Shenyang Pharmaceutical University. Published by Elsevier B.V.
This is an open access article under the CC BY-NC-ND license
(http://creativecommons.org/licenses/by-nc-nd/4.0/)

* Corresponding authors.
E-mail addresses: xudonghang@zju.edu.cn (D. Xu), gaojianqing@zju.edu.cn (J. Gao), tianyuanzhang@zju.edu.cn (T. Zhang).
Peer review under responsibility of Shenyang Pharmaceutical University.

https://doi.org/10.1016/j.ajps.2026.101122
1818-0876/© 2026 Shenyang Pharmaceutical University. Published by Elsevier B.V. This is an open access article under the CC BY-NC-ND license (http://creativecommons.org/licenses/by-nc-nd/4.0/)

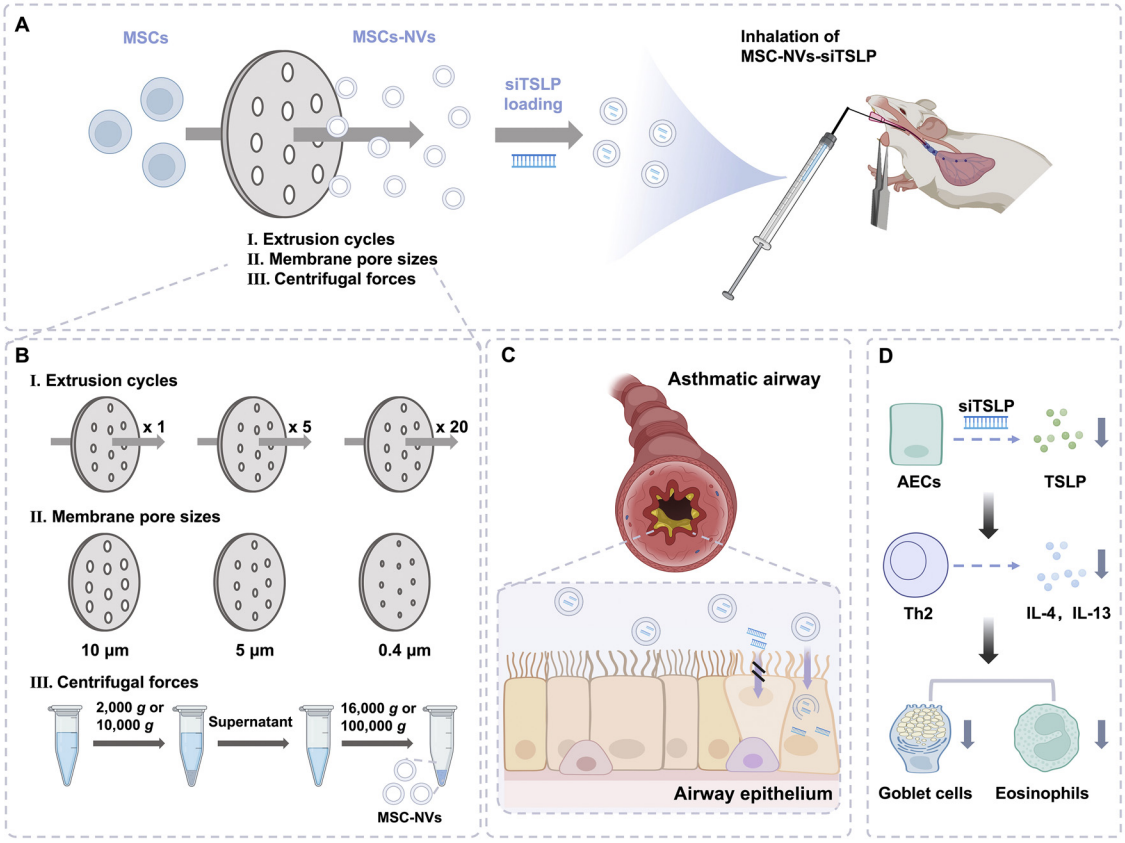
1. Introduction

Asthma, one of the most prevalent chronic inflammatory diseases, is distinguished by varying degrees of airway inflammation, obstruction, mucus hypersecretion and airway hyperresponsiveness [1]. Currently, asthma affects over 300 million individuals globally, with a continuously escalating incidence rate [2]. Conventional therapeutic approaches, including the administration of bronchodilators and anti-inflammatory medications, offer only symptomatic relief and fail to impede the progressive decline in pulmonary function characteristic of asthmatic individuals [3]. Meanwhile, prolonged use of hormonal anti-inflammatory drugs may induce adverse effects such as hypertension, diabetes and central obesity [4]. Therefore, the development of novel treatment strategies to effectively intervene in asthma progression is urgently required for clinical practice.

Recent studies have revealed that the pathogenesis of asthma is closely related to the dysregulation of interleukin (IL)-33, thymic stromal lymphopoietin (TSLP), and growth stimulation expressed gene 2 (ST2) in airway epithelial cells (AECs) [5]. Therefore, the treatment of asthma using gene therapy has attracted increasing attention. In particular, small interfering RNA (siRNA) therapy, which specifically diminishes or silences the expression of disorder genes, has shown great potential in the treatment of various immune and pulmonary disorders [6,7], and is also considered one of the most promising strategies for asthma intervention [8]. For example, TSLP is an upstream cytokine secreted by AECs upon exposure to pathogenic stimuli [9]. Downregulating TSLP can intercept inflammatory pathways at an early stage, potentially providing a more effective intervention in the early progression of the disease [10]. Importing exogenous siRNA to target critical asthmatic pathways thus constitutes a highly promising therapeutic strategy. However, the effective delivery of siRNA to AECs is currently a challenge. Systemic administration is the most reported approach for RNA molecule delivery. However, its limited accumulation at the target site, excessive hepatic uptake, and rapid clearance hinder its effectiveness in airway delivery [11–13]. Pulmonary delivery through inhalation has been proposed as an alternative approach for RNA molecule delivery to treat respiratory diseases [14,15]. Compared to systemic administration, inhalation offers several advantages, including reduced dosage, enhanced patient compliance, and minimized systemic exposure [16]. Nevertheless, the inherent instability of RNA molecules, which are susceptible to rapid enzymatic and non-enzymatic degradation, as well as their poor cell membrane penetration ability, diminishes the possibility of direct inhalation of siRNA [11]. Therefore, developing a carrier that can protect siRNA from rapid degradation *in vivo* and is suitable for inhalation is essential to overcome these challenges.

Extracellular vesicles (EVs) are natural vesicles secreted by cells that have recently been shown to serve as inherent carriers for delivering various biological signaling molecules, including small RNAs [17,18]. Due to their low immunogenicity and minimal toxicity, EVs hold significant potential for therapeutic applications [19,20]. Several pioneers have proposed their applications as a delivery system for RNA molecules [21,22], showing their inherent biocompatibility and potent transfection ability. In particular, EVs have demonstrated feasibility for inhalation-based administration, making them a promising carrier for pulmonary delivery [23]. However, the practical applications of EVs as pharmaceutical preparations face challenges, particularly the high cost related to the collection and purification of EVs from cellular supernatants, and the scale-up applications, due to their relatively low yields [24]. Thus, several strategies have been developed to overcome these limitations. Among these, the extrusion strategy, which utilizes a microfiltration technique to extrude cells sequentially and prepare EV-like nanovesicles, has elicited considerable attention [25]. The microfiltration technique was initially applied in liposome preparation and later utilized to prepare biological nanovesicles extruded from cells [26]. This method possesses the obvious advantage of producing nanovesicles with high yields, reportedly more than 20 times those of naturally produced EVs [27]. Therefore, these nanovesicles extruded from cells have been regarded as a potential replacement for EVs as a drug delivery carrier. Nevertheless, limited studies have investigated the detailed impacts of the extrusion process, including the extrusion cycles, membrane pore sizes, and centrifugal forces used for vesicle separation and purification, on the characteristics and yields of acquired nanovesicles, which is critical for their therapeutic applications. Additionally, different extrusion processes and conditions have been reported for nanovesicle preparation, however, limited studies have summarized the contributions of these differences. Therefore, a systematic study to address this issue is necessary and beneficial for further development in this field. Moreover, recent studies have suggested that some membrane proteins inherited from the parental mesenchymal stem cells (MSCs), such as CD9 and CD63, may facilitate the cellular uptake of nanovesicles [28]. Specifically, CD9 has been implicated in the initial adhesion of EVs to recipient cell membranes, while CD63-enriched vesicles preferentially interact with caveolae-rich plasma membrane regions, promoting endocytosis [29]. These molecular features may partially contribute to the enhanced internalization efficiency of MSC-derived artificial nanovesicles (MSC–NVs) during delivery.

To this end, the present study aims to develop inhalable MSC–NVs for an effective delivery of TSLP-targeted siRNA (siTSLP) into AECs, thereby controlling the asthma symptoms by alleviating airway inflammation and hyperresponsiveness. MSCs are well known for their immunomodulatory properties, which can be inherited by the EVs they produce [30,31]. For example, we have previously demonstrated that MSC-derived EVs also exhibit therapeutic potential in the treatment of spinal cord injury, partly through their immunomodulatory properties [32,33]. Similarly, artificial nanovesicles derived from MSCs are also anticipated to retain these inherent advantages [34]. In the case of asthma, this implies that MSC–NVs not only function as efficient carriers for siRNA delivery but may also directly participate in the mitigation of airway inflammation and hyperresponsiveness [35]. These dual functionalities of siRNA encapsulation and intrinsic immunomodulatory activity make MSC–NVs a highly promising therapeutic strategy for asthma and



Scheme 1 – Schematic illustration of MSC–NVs extruded from MSCs using a liposome extruder coupled with a sequential of microfilters for delivering siRNA to alleviate asthma symptoms *via* nebulized delivery. (A) Primary parameters in the extrusion process of MSC–NVs and the nebulized administration of MSC–NVs-siRNA; (B) Three main factors and their respective levels in the extrusion process; (C) MSC–NVs deliver siRNAs to AECs following pulmonary administration; (D) RNA interference mechanism reduces TSLP levels, thereby inhibiting Th2 cytokine production, eosinophil infiltration, and goblet cell metaplasia.

other inflammation-associated respiratory diseases. To optimize the preparation of MSC–NVs with high yields and suitability for inhalation, impacts of each critical parameter in the extrusion processes were systematically studied and optimized through the orthogonal tests. Also, the protection of siTSLP during the nebulization, as well as the delivery capability of siTSLP towards airways and lungs by MSC–NVs were examined. At last, the therapeutic potential of siTSLP-loaded MSC–NVs (MSC–NVs-siTSLP) in mice models with ovalbumin-induced asthma symptoms through inhalation administration was investigated (Scheme 1). It is expected that the present work will show the possibilities and effectiveness of treating asthma through the inhalable administration of therapeutic RNAs using stem cell-derived artificial nanovesicles, and thereby providing a promising delivery platform for treating asthma and potentially other respiratory diseases. Compared with most synthetic nano-preparations, MSC–NVs show the advantages of intrinsic immunomodulatory properties inherited from their parent MSCs, thereby achieving a synergistic therapeutic effect in suppressing asthma pathogenesis. Moreover, the impacts of different extrusion parameters on the characteristics and performance of prepared MSC–NVs may act as a guide for the further preparation and optimization of man-made nanovesicles.

2. Material and methods

2.1. *Materials*

Tris-Gly protein gels (5%–20%), western blot transfer buffer, loading buffer, Tris-buffered saline containing Tween (TBST), polyvinylidene fluoride (PVDF), LysoTracker green, 1,1'-dioctadecyl-3,3,3',3',-tetramethylindodicarbocyanine(DiD), 4',6-diamidino-2-phenyl indole (DAPI), and Hoechst dye 33342 were purchased from Beyotime (Shanghai, China). siRNA targeting GAPDH (siGAPDH), negative control siRNA (siNC), Cy5-labeled siRNA (Cy5-siRNA), and siRNA targeting TSLP (siTSLP) were procured from GenePharma (Shanghai, China). CD105, CD63, CD9, TSG101 and β-actin antibodies were provided by Abcam (Cambridge, UK). Bronchial epithelial cell medium for BEAS-2B cells was obtained from Zhong Qiao Xin Zhou Biotechnology (Shanghai, China). Fibroblast growth factor (FGF) and epidermal growth factor (EGF) were purchased from Pepro Tech (Cranbury, USA). Minimum essential medium

α (α-MEM) culture medium was purchased from VivaCell Bioscience (Shanghai, China). GelRed, Tris-borate-EDTA buffer (TBE), triton X-100, and RNase A were procured from Beyotime (Shanghai, China). Fetal bovine serum (FBS) was provided by Gibco (New York, USA). Mouse IL-6, IL-1β, TNF-α, IL-4, IL-13 and TSLP enzyme-linked immunosorbent assay (ELISA) kits were purchased from LiankeBio (Hangzhou, China). RNA rapid extraction solution, SweScript all-in-one RT SuperMix, and universal blue SYBR green qPCR master mix were provided by Servicebio (Wuhan, China). Ovalbumin (OVA), aluminium adjuvant, goat anti-mouse IgG (H + L) secondary antibody and micro bicinchoninic acid (BCA) protein assay kit were purchased from Thermo Fisher Scientific (Waltham, USA). Collagenase I and DNase I were obtained from Yeason (Shanghai, China). MC3-LNP-siRNA was obtained from GenScript (Nanjing, China).

The MSCs derived from human umbilical cord blood were sourced from SinoCell Co., Ltd. (Ningbo, China) under ethics approval No. 2021-R108 (Ningbo First Hospital MRC, China). and all procedures complied with international ethical guidelines. BEAS-2B human lung epithelial cells (ZQ0381) were procured from ScienCell Research Laboratories (Shanghai, China). α-MEM medium containing 10% FBS, FGF and EGF (each at 10 ng/mL) was used for MSC expansion, and MSCs within passages 6–10 were selected for all subsequent experiments. BEAS-2B cells were propagated in dedicated airway epithelial basal medium. Cell cultures were sustained under standard conditions: 37°C in a humidified incubator with 5% CO_2.

Female Balb/c mice (six weeks old) and male ICR mice (22–24 g) were purchased from SLAC Laboratory Animal Co., Ltd. (Shanghai, China). The Animal Experiments Ethics Committee of Zhejiang University (approval No. ZJU20241043) reviewed and authorized all animal studies, which strictly complied with institutional animal welfare protocols.

2.2. *Preparation of MSC–NVs*

MSCs were harvested via trypsinization and resuspended in phosphate-buffered saline (PBS). The cell density was adjusted to about 1.5×10^6 cells/ml. Next, the cell suspension was extruded through a series of nanopore-sized polycarbonate membrane filters (Whatman, UK) using a LiposoFast (Avestin, Canada). The extruded solution was then collected and centrifuged for 30 min at 4°C under a centrifugal force of 2000 g or 10,000 g, and the precipitation was discarded to remove most cell fragments and apoptotic bodies. The supernatant was again centrifuged at 16,000 g or 100,000 g for 60 min, and the precipitate was collected to obtain nanovesicles. The micro BCA protein assay kit was then used to measure the total protein content of the isolated nanovesicles.

2.3. *Characterization of MSC–NVs*

The morphology of MSC–NVs was imaged via a transmission electron microscope (TEM) (Talos, Thermo Scientific, USA) at 120 kV. Prior to visualization, the nanoparticle concentration was adjusted to 100 μg/ml. A 5-μl aliquot of the MSC–NV suspension was deposited on a carbon-coated copper grid for 60-s adsorption, followed by staining with 2% uranyl acid ester (5 μl). Physicochemical characterization of MSC–NVs, including hydrodynamic diameter and surface charge properties (zeta potential), was performed using the Zetasizer Nano ZS90 analytical system (Malvern, USA).

2.4. *Preparation of MSC–NVs-siRNA*

The siRNA was encapsulated into MSC–NVs using an Exo-Fect exosome transfection kit (System Bioscience, USA), which can facilitate the internalization of target siRNA into the nanovesicles with the assistance of a cell-penetrating peptide. Briefly, purified MSC–NVs (≈ 50–300 μg protein) were mixed with Exo-Fect reagent (10 μl) and siRNA (20 pmol) in PBS to a final reaction volume of 150 μl, incubated at 37 °C for 10 min, and then placed on ice. The reaction was stopped with ExoQuick-TC reagent, followed by centrifugation to remove free siRNA, and the pellet was resuspended in PBS for subsequent experiments.

2.5. *Encapsulation efficiency*

The encapsulation of siRNA in MSC–NVs was first quantified as the siRNA load per particle by measuring the fluorescence intensity of Cy5-siRNA using a microplate reader (excitation wavelength = 645 nm, emission wavelength = 685 nm). Cy5-siRNA was serially diluted in PBS to the following concentrations: 1 μM, 500 nM, 250 nM, 125 nM, 62.5 nM, 31.3 nM, 15.6 nM, 7.8 nM, 3.9 nM, 2.0 nM, 1.0 nM with a volume of 100 μl for each dilution, and 0 nM was set as the control group. Subsequently, 80 μl of each diluted Cy5-siRNA and an equivalent volume of appropriately diluted nanovesicle samples loaded with siRNA were added to the wells of a black 96-well plate. Fluorescence intensity was measured using a microplate reader. The serially diluted Cy5-siRNA was used to generate a fluorescence intensity-concentration standard curve, which was then applied to calculate the total amount of siRNA loaded in the nanovesicle samples based on their measured fluorescence. Simultaneously, the particle number of the vesicles was quantified using nano-flow cytometry (N30, NanoFCM, China), allowing calculation of the final siRNA loading per vesicle. siRNA load per particle = (Concentration of siRNA calculated by substituting the sample fluorescence values into the standard curve × dilution factor during fluorescence detection × total volume of the exosome sample after loading)/Total amount of exosomes after loading. In addition, the overall encapsulation efficiency was evaluated by comparing the fluorescence intensity of the total input Cy5-siRNA with that of the free Cy5-siRNA remaining in the supernatant after the encapsulation process. The encapsulation efficiency was calculated using the following formula: Encapsulation efficiency (%) = (Fluorescence intensity of total Cy5-siRNA input - Fluorescence intensity of free Cy5-siRNA in the supernatant)/Fluorescence intensity of total Cy5-siRNA input × 100%.

2.6. *Encapsulation and protective effect of MSC–NVs*

The siRNA encapsulation efficiency and protective capacity of MSC–NVs were evaluated using agarose gel electrophoresis.

MSC–NVs-siRNA complexes were treated with Triton X-100 or PBS and underwent electrophoretic verification using GelRed-stained 1% agarose gel. Constant voltage electrophoresis at 150 V for 20 min in TBE buffer enabled visualization of nucleic acid retention patterns, serving as validation of encapsulation. To evaluate the siRNA protection capacity of MSC–NVs, samples were incubated with RNase A or PBS (control) at physiological temperature (37°C) for 30 min and subjected to subsequent Triton X-100 lysis prior to electrophoretic verification.

2.7. *Observation of the* in vitro *cellular uptake*

BEAS-2B cells were seeded in confocal dishes (1×10^5 cells/dish) under standard culture conditions (37 °C, 5% CO_2) for 12 h to allow adherence. Next, comparative exposure of cells to MSC–NV-Cy5-siRNA and free Cy5-siRNA was conducted for 4 h. Post-incubation cellular processing involved the following sequential steps: (1) removal of cell culture medium, (2) PBS washing cycles, (3) lysosomal labeling with LysoTracker (1:20,000) for 30 min, and (4) nuclear counterstaining with Hoechst dye. Subcellular localization patterns were captured via a confocal laser scanning microscopy (CLSM) imaging system (Leica LAS X, Leica, Germany).

2.8. *Determination of cellular uptake efficiency* in vitro

The cellular uptake capacity of BEAS-2B cells for MSC–NVs-Cy5-siRNA (before or after nebulization) was quantitatively assessed through flow cytometry (BD Biosciences, USA). Cells were initially plated in 12-well culture dishes (1×10^5 cells/well) for 24 h before exposure. Following 4 h of coculture with nanovesicles under physiological conditions (37 °C, 5% CO_2), cellular suspensions were resuspended in 500 µl PBS prior to flow cytometry. Cy5-positive BEAS-2B cells were then gated to assess siRNA internalization rates.

2.9. *Determination of the gene silencing effect in real-time PCR (RT-PCR)*

To assess siRNA delivery efficacy in BEAS-2B cells, MSC–NVs carrying siGAPDH were selected as the experimental model. Cells were cultured in six-well dishes (1.5×10^5 cells/well) for 24 h. Subsequently, cultures were exposed to MSC–NVs loaded with siGAPDH or negative control siRNA (siNC) for 48 h, with PBS and unencapsulated siGAPDH serving as the blank and negative control. RNA isolation was conducted using a commercial extraction kit with standard protocols. Reverse transcription employed SweScript RT reagents, followed by SYBR green-based qPCR quantification after normalization with β-actin. The relative expression levels of target mRNA were calculated using the $2-\Delta\Delta CT$ analytical approach. Primer sequences were: GAPDH-S (5′-GGAAGCTTGTCATCAATGGAAATC-3′), GAPDH-A (5′-TGATGACCCTTTTGGCTCCC-3′); ACTIN-S (5′-CACCCAGCACAATGAAGATCAAGAT-3′), ACTIN-A (5′-CCAGTTTTTAAATCCTGAGTCAAGC-3′).

2.10. *Determination of the gene silencing effect in western blot assay*

The GAPDH silencing effect mediated by MSC–NVs-siGAPDH complexes was further validated by western blot analysis. BEAS-2B cells were plated in six-well culture dishes at 1.5×10^5 cells/well. Following a 24-h adherence period, cellular monolayers were exposed to either MSC–NVs-siGAPDH or MSC–NVs-siNC for 48 h, with equivalent PBS and naked siGAPDH treatments serving as the blank and control, respectively. Cell lysates were prepared using RIPA buffer following harvest procedures. Protein quantification was performed using the BCA assay. Proteins were denatured using electrophoresis loading buffer, separated by SDS-PAGE (10% gel), and transferred onto PVDF membranes. The membranes were subsequently blocked with 5% non-fat milk/TBST for 1 h and incubated overnight at 4 °C with primary antibodies (1:10,000). After TBST washing cycles, membranes were incubated with HRP-linked secondary antibodies (1:5,000) at ambient temperature for 1 h. Target protein bands were visualized via enhanced chemiluminescence detection using a gel imaging system (Bio-Rad, USA), with β-actin serving as the housekeeping control.

2.11. *Mouse model of asthma*

Female BALB/c mice were sensitized using intraperitoneal injection of 200 µl OVA-aluminum adjuvant (80 µg) on Day 0 and Day 14, while control mice were injected with equivalent saline injections. 5–7 d later, the sensitized mice were exposed to 1.5% OVA aerosol for 40 min/d for 3 d consecutivly using a nebulizer (Omron, China). Tissues were harvested 24 h after the final exposure for further analysis.

2.12. *Biodistribution study*

Asthmatic mice were euthanized at predetermined intervals post-MSC–NVs-Cy5-siRNA nebulization for multi-organ imaging via the IVIS platform (Caliper PerkinElmer, USA). Pulmonary cell targeting analysis involved enzymatic dissociation: excised lungs were mechanically fragmented and subjected to collagenase I (2 mg/ml)/DNase I (50 U/ml) digestion in PBS at 37 °C for 1 h. After digestion, suspensions were sequentially filtered through 70 µm and 40 µm meshes, followed by erythrocyte lysis (10 min) and centrifugation (2,800 rpm). Cell resuspensions were stained with fluorochrome-conjugated antibodies against EpCAM-APC/cyanine7 (epithelial cells), CD45-PerCP/Cy5.5 (immune cells), and CD31-AF488 (endothelial cells) for 30 min at 4 °C. Cellular internalization profiling was performed using flow cytometry (BD Biosciences, USA). The detailed gating strategy for $Cy5^+$ cell populations is provided in Fig. S1.

2.13. *Treatment of asthmatic mice*

On Day 21, asthmatic mice received intratracheal administration via a pressure nebulizer with either MSC–NVs, MSC–NVs-siNC, or MSC–NVs-siTSLP (50 µl per mouse containing 20 µg MSC–NVs). The PBS-treated group (50 µl

per mouse) was set as the negative control. Lung tissues and biological samples were collected for subsequent analysis 24 h after the final OVA/PBS challenge.

2.14. *Determination of immune cells and inflammatory cytokines*

The quantification of TSLP, IL-4 and IL-13 concentrations in the supernatant of lung homogenate was performed using ELISA following the manufacturer's protocols. The immune cells collected from bronchoalveolar lavage fluid (BALF) were suspended in 0.5 ml PBS, and white blood cell counts and eosinophil ratios were obtained by routine blood examination.

2.15. *Determination of lung histology*

Left lung specimens were fixed in 4% paraformaldehyde for 24 h for histopathological evaluation. Paraffin-embedded lung sections (5 μm) were subjected to hematoxylin-eosin (H&E) and periodic acid-Schiff (PAS) staining to assess inflammatory infiltrates and mucus-producing cell proliferation, respectively.

2.16. *Biosafety evaluations*

Healthy ICR mice were used to preliminarily evaluate the potential risks of MSC–NVs and MSC–NVs-siRNA. In brief, mice were administered with MSC–NVs and MSC–NVs-siRNA on Day 1 and again on Day 3. Systemic blood acquisition was performed via a retro-orbital approach for complete blood count evaluation. Lungs were collected and sectioned for pathological examination after H&E and immunohistochemical staining. Inflammatory cytokine levels (IL-6, IL-1β and TNF-α) and immune cell populations isolated from BALF were also analyzed.

2.17. *Statistical analysis*

Data processing was conducted using GraphPad Prism 10 (GraphPad Software, LLC). Results from triplicate experiments are reported as means ± standard deviation (SD). Intergroup comparisons utilized a two-tailed Student's *t*-test for two groups and ordinary one-way or two-way analysis of variance (ANOVA) for multiple groups.

3. Results and discussion

3.1. *Preparation and optimization of MSC–NVs using extrusion method*

As depicted in Fig. 1A, MSC–NVs were prepared using sequential extrusion method referred by a previous report [27], which involved extruding MSCs through polycarbonate membrane microfilters with defined pore sizes, followed by ultracentrifugation for separation and purification. Furthermore, in order to figure out the impact of critical extrusion parameters on the characteristics and yield of the prepared vesicles, an orthogonal experimental design was applied to identify the optimal extrusion process for MSC–NV preparations. Herein, three primary parameters and some commonly used levels in the extrusion process were selected [24,36], including extrusion cycles, membrane pore sizes, and centrifugal forces. The extrusion cycles were set at 1, 5, 10 and 20 cycles. The polycarbonate membrane pore sizes included 10 μm, 5 μm and 0.4 μm, including passing through a single pore size membrane and sequentially through two or three pore sizes. Specifically, these were the six groups established: 10 μm, 5 μm, 10–5 μm, 10–0.4 μm, 5–0.4 μm, and 10 to 5 to 0.4 μm. The 0.4-μm pore size was excluded from the single pore size group due to its small size, which prevented successful extrusion. Additionally, four combinations of centrifugal forces were tested, and the centrifugation process was divided into two steps: the first step aimed to remove cell debris and large vesicles, while the second step was used to purify and collect vesicles. The first step was set at either 2000 g or 10,000 g, and the second step at either 16,000 g or 100,000 g. This resulted in four combinations, which were as follows: 2000 g and 16,000 g, 2000 g and 100,000 g, 10,000 g and 16,000 g, and 10,000 g and 100,000 g.

To systematically optimize the extrusion process, this study focused on three primary factors in the extrusion process by employing a three-factor, three-level orthogonal design. Initially, single-factor experiments were conducted to screen three optimal levels for each factor. The particle size, polydispersity index (PDI), and yield of MSC–NVs served as the primary evaluation criteria due to their critical relevance for MSC–NVs applications as delivery vehicles. First, precise control over particle size is essential for the effective nanovesicles-based delivery to target cells. Generally, nanovesicles with diameters of 50–200 nm exhibit superior cellular uptake, particularly in inflammatory microenvironments where endocytosis is enhanced [29]. In contrast, particles exceeding 200 nm are more likely to be recognized and engulfed by phagocytic cells, such as macrophages, leading to rapid clearance and reduced delivery efficiency [37]. Furthermore, the uniformity of the prepared nanovesicles, as indicated by a low PDI, is crucial for ensuring consistent performance and reproducibility in therapeutic applications. The oversized particles may become trapped in mucus and be rapidly cleared, while extremely small ones can leak into blood vessels through lung tissue, compromising therapeutic efficacy. A PDI range of 0.1–0.3 is generally considered optimal for moderate dispersity [38]. Moreover, extrusion processes with higher yields enable more cost-effective production, thus holding compelling advantages for practical applications that requires a highly efficient manufacturing pathways. In present study, the vesicle count was used as the primary indicator of MSC–NV yield, with the quantification of protein versus particle count demonstrated in Fig. S2. MSC–NVs As shown in Fig. 1B, MSC–NVs had an average particle size of around 200 nm across different extrusion cycles. The PDI showed a consistent value of around 0.3. In contrast, yield of MSC–NVs exhibited statistically significant differences: single-time extrusion generated the lowest yield, while 20 cycles produced the highest output, reaching twice that of the single-time group. Similarly, single-factor experiments on the remaining parameters showed analogous findings: particle sizes predominantly fell within the 50–200 nm target range, with no significant intergroup

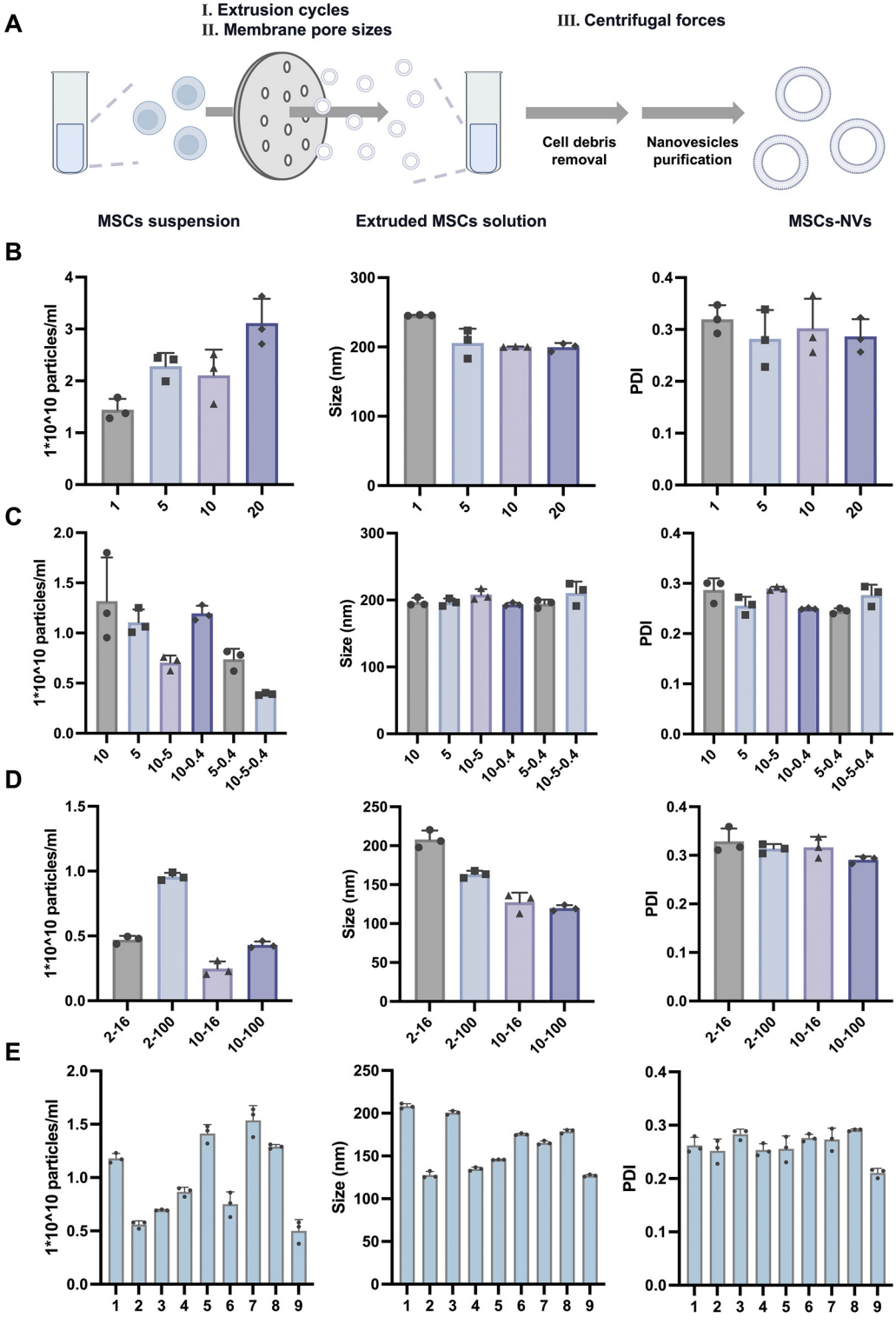


Fig. 1 – Optimization of the extrusion process for yield maximization and particle size regulation using orthogonal experiment. (A) Schematic illustration demonstrating the extrusion process. Impact of (B) extrusion cycles, (C) membrane pore sizes, and (D) centrifugal forces on MSC–NV yield, particle size and PDI ($n = 3$). (E) Yield, particle size and PDI of the nine parallel groups obtained through the orthogonal design ($n = 3$). Data are presented as the means ± SD.

differences in PDI (all around 0.3), while yields exhibited statistically significant differences. Therefore, the yield was selected as the primary criterion to identify the three optimal levels for each factor in MSC–NV preparation (Fig. 1C and 1D). The three yield-optimized levels for each parameter comprised extrusion cycles (5, 10 and 20 cycles), membrane pore sizes (10 μm, 5 μm, and 10–0.4 μm), and centrifugal forces (2000 g and 16,000 g, 2000 g and 100,000 g, and 10,000 g and 100,000 g).

Next, the orthogonal experiment was conducted with three factors at three levels (Table S1), resulting in nine parallel groups. The particle size, PDI, and yield were evaluated after extrusion under each group's conditions (Fig. 1E). It was observed that the average particle size was within a reasonable range, with no significant intergroup differences in PDI (all data below 0.3), while the yield varied significantly. Among all parallel groups, group 7 exhibited the highest yield, reaching approximately 1.5×10^{10} particles/ml. Based on the number of MSCs consumed, the yield was about 3×10^9 particles per 10^6 cells. Therefore, yield was then applied as the evaluation criterion, and the results of the orthogonal experiment were analyzed using the range analysis. Thus, the order of influence of each factor on yield was as follows: centrifugal forces, membrane pore sizes, and extrusion cycles. The optimal extrusion condition was identified as extrusion through a 10 μm polycarbonate membrane for 20 cycles, followed by separating and purifying under centrifugal forces of 2000 g and 100,000 g (Table S2). Moreover, the results of the variance analysis verified that the centrifugal force combination had the most significant impact on MSC–NVs yield (Table S3). In summary, the systematic evaluation of three critical extrusion parameters demonstrated that optimized processing enhanced MSC–NVs yield, while the particle size ($\sim$ 150 nm) and PDI ($\sim$ 0.25) fell well within the nebulization-compatible ranges (50–200 nm for particle size and PDI $<$ 0.3), making the resulting MSC–NVs suitable for inhalation delivery. It should be noted that while potential interactions between extrusion parameters were not explicitly analyzed, the observed consistency of vesicle size and PDI across all tested conditions suggests minimal impact of such interactions on the suitability of MSC–NVs for nebulized delivery. Future studies may further explore these interactions to refine process optimization, particularly in the context of large-scale production.

3.2. *MSC–NVs act as efficient vehicles for siRNA loading and delivery*

To enhance intervention in the early progression of asthma, MSC–NVs were used to load and deliver siTSLP (Fig. 2A). As shown in Fig. 2B, under Exo-Fect transfection conditions, MSC–NVs achieved efficient siRNA encapsulation, with an impressive loading capacity exceeding 600 siRNA molecules per particle. In addition, the encapsulation efficiency analysis demonstrated a superior loading capacity for siTSLP, which the encapsulation rate was 91.6% ± 5.5%. Using PBS as a control, agarose gel electrophoresis revealed the siRNA band only after treatment with Triton X-100, an amphiphilic surfactant known to disrupt biological membranes (Fig. 2C), confirming successful siRNA encapsulation within MSC–NVs. Furthermore, the MSC–NVs-siRNA and free siRNA were separately treated with RNase A. Results showed that free siRNA was degraded after RNase A treatment, while the siRNA encapsulated in MSC–NVs remained protected from enzymatic degradation (Fig. 2D). Furthermore, efficient cellular uptake is critical to ensure the successful execution of siRNA-mediated gene silencing. Thus, the BEAS-2B human bronchial epithelial cell line was adopted for *in vitro* experiments and treated with both naked siRNA and encapsulated siRNA in MSC–NVs. The cellular internalization of free siRNA was almost undetectable, whereas siRNA delivered *via* MSC–NVs was obviously taken up by the cells. Furthermore, the fluorescence signals of siRNA and LysoTracker green-labeled lysosomes exhibited minimal overlap, indicating that the encapsulated siRNA successfully escaped from lysosomal entrapment post cellular internalization (Fig. 2E). This efficient lysosomal escape may be partially attributed to MSC–NVs as natural vesicles and their ability to mediate membrane fusion [39].

To further validate the gene silencing effect of siRNA following cellular uptake, siGAPDH, targeting GAPDH, was employed as a model gene to evaluate its impact on mRNA and protein expression levels using qPCR and western blot assay, respectively. With the PBS group serving as a control, free siGAPDH exhibited no significant effect on mRNA levels or protein expression, aligning with our previous observation that free siRNA can hardly be internalized by cells. Similarly, siNC delivered by MSC–NVs did not knock down the expression of GAPDH at either the gene or protein level. In contrast, MSC–NVs-siGAPDH markedly reduced mRNA and protein levels by approximately 50% compared to the control group (Fig. 2F and 2G). Thus, these findings confirm that the gene silencing effect is specifically mediated by siRNA delivered *via* MSC–NVs.

3.3. *MSC–NVs can be nebulized with limited impact on their structural integrity and siRNA delivery capability*

Nebulized inhalation of siRNAs holds several advantages for the treatment of respiratory diseases, such as lung-specific targeting, sustained high local concentrations, and minimized systemic side effects [19,40]. Here, the feasibility of administering MSC–NVs *via* inhalation using a pressure nebulizer was further explored. In particular, the primary characteristics and siRNA leakage of MSC–NVs post-nebulization were examined, considering the intense shear forces generated during the nebulization process might impact their structural integrity and delivery capability. As presented in Fig. 3A, TEM images revealed that MSC–NVs exhibited the typical "cup-shaped'' morphology before nebulization and retained their intact spherical structure following nebulization. This observation verifies that the nebulization process does not compromise the structural integrity of the nanovesicles, which is essential for maintaining the functionality of MSC–NVs as effective carriers for siRNA delivery. Moreover, the average particle size (Fig. 3B), size distribution (Fig. 3C), and PDI (Fig. 3D) of MSC–NVs showed no significant differences before and after nebulization. The zeta potential post-nebulization was also observed to be consistent with that prior to nebulization (Fig. 3E). In addition,

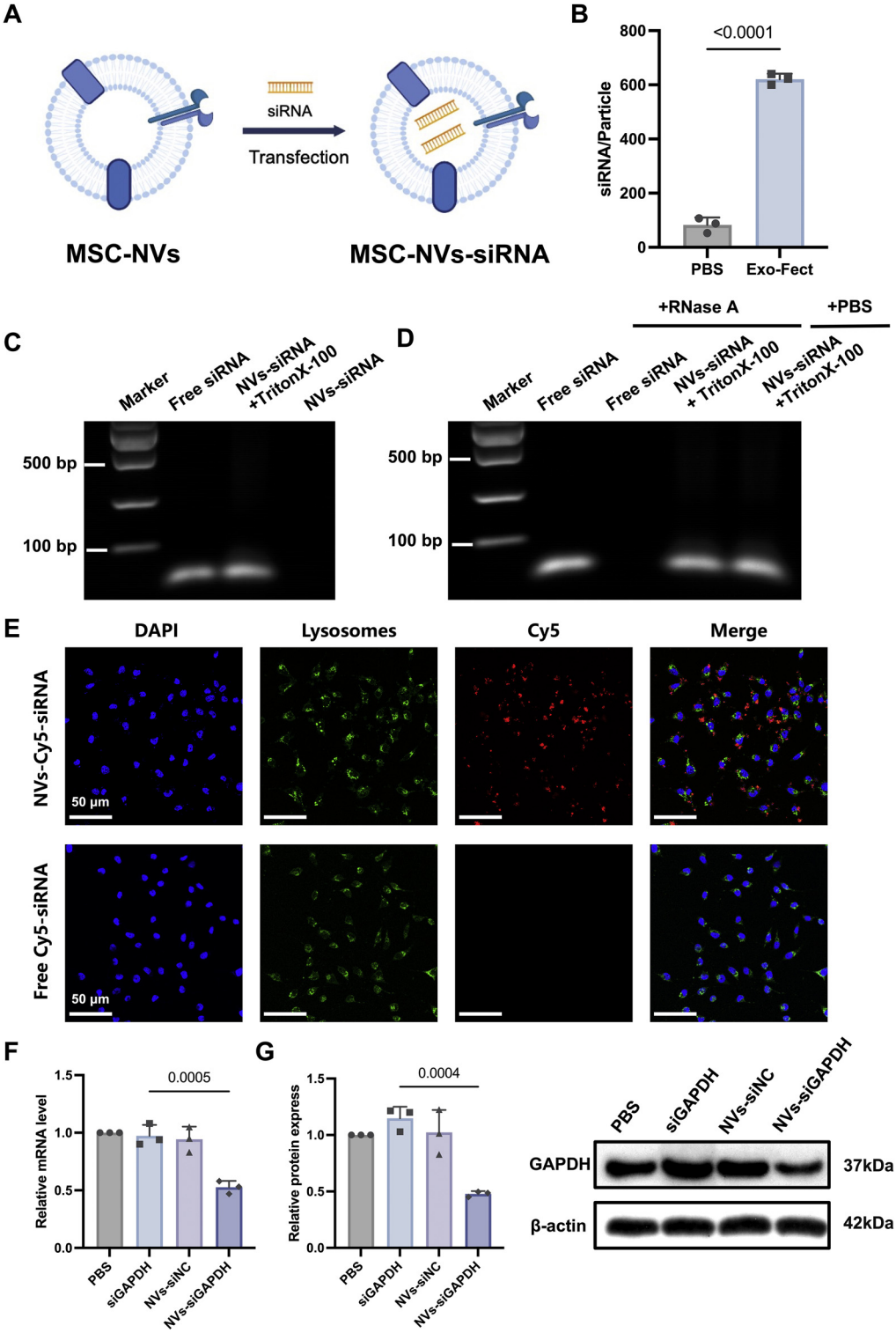


Fig. 2 – Successful loading of siRNA in MSC–NVs for efficient gene silencing of BEAS-2B cells. (A) Schematic illustration of siRNA loading by MSC–NVs. (B) The number of siRNA molecules encapsulated per nanovesicle under Exo-Fect treatment, quantified using fluorescence-based analysis ($n = 3$). (C) Agarose gel electrophoresis of MSC–NVs-siRNA after treatment with or without Triton X-100. (D) Protective ability of MSC–NVs against siRNA degradation by RNase A. (E) Intracellular distribution of Cy5-siRNA in BEAS-2B cells. siRNA was stained with Cy5 (red), the nucleus was stained with DAPI (blue), and lysosomes were stained with LysoTracker (green). Scale bar = 50 μm. Relative (F) mRNA levels based on RT-PCR and (G) protein expression levels based on western blot assay in BEAS-2B cells ($n = 3$). Data are presented as the means ± SD. Statistical significance was calculated using the *t*-test in (B) or ordinary one-way ANOVA in (F, G). The *P*-value indicates the statistical difference between the groups.

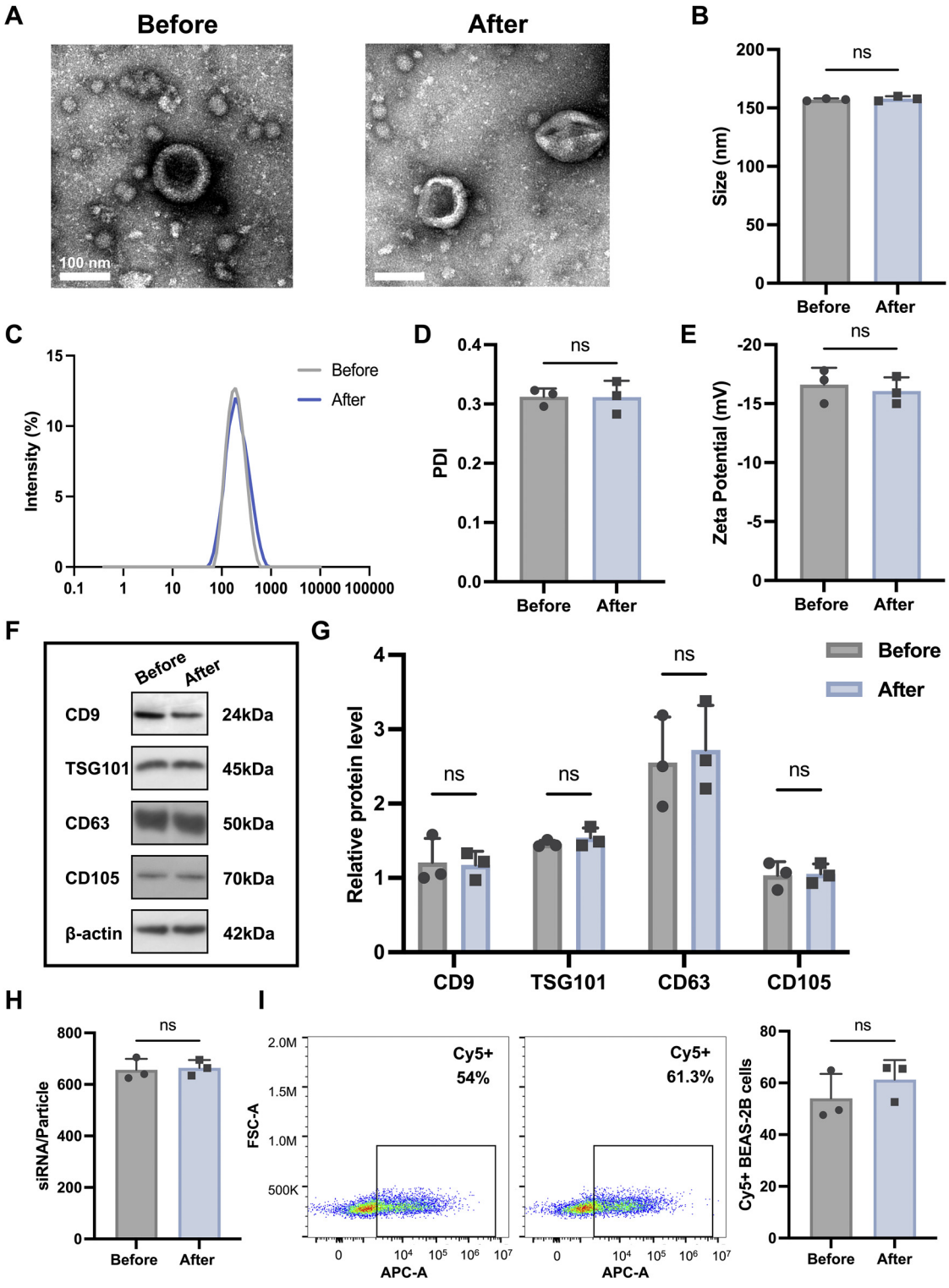


Fig. 3 – Characterization and drug delivery capacity of MSC–NVs before and after nebulization. (A) TEM images of MSC–NVs before and after nebulization. Scale bar: 100 nm; Stability of (B) average particle size, (C) size distribution, (D) PDI and (E) surface charge of MSC–NVs ($n = 3$); (F) Western blot images showing CD9, TSG101, CD63 and CD105 protein levels on MSC–NVs before and after nebulization; (G) Quantitative analysis of CD9, TSG101, CD63 and CD105 expression normalized to β-actin ($n = 3$); (H) siRNA encapsulation capacity of MSC–NVs before and after nebulization ($n = 3$); (I) Impacts of the nebulization process on cellular uptake of MSC–NVs-siRNA in BEAS-2B cells ($n = 3$). Data are presented as the means ± SD. Statistical significance was calculated using the *t*-test in (B, D, E, H, I) or ordinary two-way ANOVA in (G). ns indicates no statistical difference between the groups.

surface marker proteins of MSC–NVs, including CD9, TSG101, CD63 and CD105, are commonly utilized for identifying various vesicle types and are involved in vesicle formation and function as delivery vehicles [27,41,42]. As shown in Fig. 3F and G, the expression levels of these proteins remained unchanged before and after nebulization, suggesting that the nebulization process had a limited adverse impact on membrane proteins. Furthermore, the effect of the nebulization process on the encapsulation of siRNA within MSC–NVs was investigated. The Cy5-labeled siRNA was loaded into MSC–NVs and subjected to nebulization to investigate the leakage of these siRNAs. As shown in Fig. 3H, a minimal leakage of siRNA was observed during nebulization. This observation aligns with the prior TEM images, which confirmed that the structural integrity of the nanovesicles was preserved after nebulization. Thus, the particle size, zeta potential, surface proteins, and siRNA loading capacity of MSC–NVs remained unchanged after nebulization, indicating the inhalable potential of MSC–NVs. To further confirm that siRNA delivery capability was unaffected, both nebulized and non-nebulized MSC–NVs were co-cultured with BEAS-2B cells for 4 h. The delivery efficiency of Cy5-labeled siRNA was then determined by evaluating fluorescence intensities in BEAS-2B cells, showing no significant difference between the nebulized and non-nebulized groups (Fig. 3I). Furthermore, western blot analysis (Fig. S3) showed that the expression of GAPDH in BEAS-2B cells was effectively reduced by both nebulized and non-nebulized MSC–NVs-siRNA, confirming that the siRNA maintained its functionality following the nebulization. Thus, the above results collectively support the feasibility of using nebulized MSC–NVs as an effective delivery system for siRNAs without significant alterations in their structural integrity and biofunctions.

3.4. *Inhalation of MSC–NVs enables effective siRNA delivery targeting TSLP with prolonged lung retention*

Since we demonstrated the feasibility of siRNA delivery *via* nebulized MSC–NVs, the biodistribution of MSC–NVs-siRNA in the lungs after inhalation administration was investigated. As presented in Fig. 4A, the fluorescence intensity in major organs confirmed that siRNA was successfully targeted to the lungs and distributed across all pulmonary lobes, permitting the uniform delivery of siRNA into pulmonary tissues and avoiding potential side effects associated with distribution to other organs (Fig. 4B and 4C). Subsequently, the fluorescence intensities of the entire lung at 4, 24 and 48 h post-inhalation showed a time-dependent decrease in both groups (Fig. 4D). The encapsulation of siRNAs within MSC–NVs exhibited a long-time protective effect. A decrease in fluorescence intensity of naked siRNA was observed at 24 h after the initial administration compared with that of MSC–NVs, with the intensity of naked siRNA dropping below the detectable range. However, MSC–NVs-siRNA retained a fluorescence signal even at 48 h, suggesting that inhalable MSC–NVs not only facilitated the accumulation of therapeutic siRNAs in lung tissues but also prolonged their retention time. In addition, the local distribution of inhalable MSC–NVs within the lungs was studied. Cryosections of lung samples demonstrated that MSC–NVs were mainly distributed along the airways, with higher fluorescence intensity observed in the AECs along the bronchi compared to the lower airways and alveoli (Fig. 4E).

Furthermore, the major cell subtypes colocalizing with the MSC–NVs-siRNA were investigated, and the results indicated that different types of lung cells exhibited distinct uptake behaviors towards MSC–NVs-siRNA following inhalation. As presented in Fig. 4F, after inhalation, siRNA was taken up by ~12.2% of lung cells. Among these, epithelial cells demonstrated the highest siRNA uptake, reaching 13.4% (Fig. 4G and 4J), which was consistent with the higher mean fluorescence intensity (MFI) observed in the AECs from previous cryosectioned tissue samples. The second most abundant uptake of siRNAs was observed in the immune cells, with Cy5-positive (Cy5+) immune cells accounting for approximately 5% (Fig. 4G and 4H). In the microenvironment of asthmatic lung, the number of macrophages that play a central role in the clearance of nanoparticles is significantly increased [43]. However, a larger proportion of siRNA was still preferentially taken up by epithelial cells, indicating that inhalable administration facilitated MSC–NVs-siRNA uptake by AECs. Previous studies have shown that, compared to positively charged particles, negatively charged MSC–NVs are less susceptible to phagocytosis by macrophages [44]. Moreover, the average particle size of MSC–NVs, being less than 200 nm, falls outside the optimal size range (0.5–5 μm) typically targeted by alveolar macrophages for phagocytosis [45,46]. These factors collectively contribute to the limited phagocytosis of the nanovesicles by immune cells. As indicated in Fig. 4G and 4I, endothelial cells exhibited the lowest proportion of Cy5+ cells (< 5%), suggesting minimal distribution of MSC–NVs into these cells. Collectively, these results suggest that the inhalable MSC–NVs hold great promise as an AEC-targeted gene delivery system.

3.5. *Inhalation delivery of siTSLP via MSC–NVs achieves efficient asthma intervention in murine models*

Having demonstrated that MSC–NVs effectively protect encapsulated siRNA post-nebulization and mediate efficient gene silencing in BEAS-2B cells, we next sought to investigate whether inhalable MSC–NVs could serve as a delivery system for siTSLP in asthma treatment using a murine model. Mice were initially sensitized with OVA, followed by inhalation administration of MSC–NVs or MSC–NVs-siTSLP prior to continued OVA challenges. Mice were sacrificed 3 d post-treatment to evaluate the therapeutic efficiency (Fig. 5A). In pre-treatment tests, varying the administered concentrations and frequencies of inhalable MSC–NVs showed a slight impact on the expression levels of inflammatory cytokines of IL-4 and IL-13, as well as eosinophil proportions (Fig. S4). Therefore, a single inhalation dose of 20 μg was selected to optimize cost-effectiveness and for the clinical advantages of a simplified administration protocol in asthma treatment. As demonstrated in Fig. 5B, TSLP levels in lung homogenate supernatants were significantly elevated in PBS-treated asthmatic mice compared to healthy controls. Notably, administration of MSC–NVs, MSC–NVs-siNC or MSC–NVs-siTSLP significantly reduced the TSLP levels compared to the PBS treatment. Thus, MSC–NV inhalation significantly

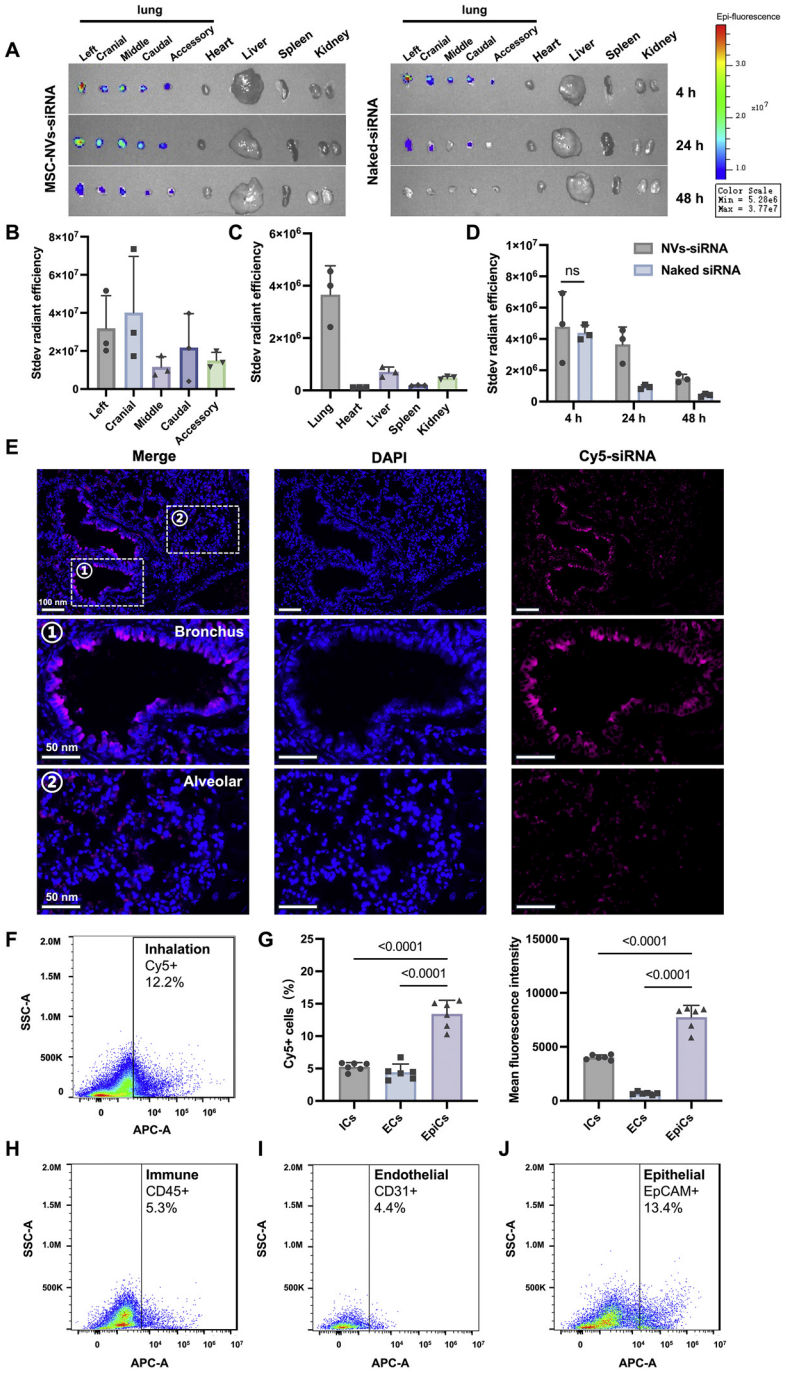


Fig. 4 – Pulmonary biodistribution of MSC–NVs-siRNA in asthmatic mice following nebulization. (A) IVIS images of lungs and other major organs collected at different time points after inhalation administration; (B) Stdev radiant efficiency of five lobes of the lungs measured using IVIS ($n = 3$); (C) Stdev radiant efficiency of lungs and other organs at 4 h after inhalation measured using IVIS ($n = 3$); (D) Stdev radiant efficiency of lungs for MSC–NVs-siRNA and naked siRNA at indicated time points measured using IVIS ($n = 3$); (E) Immunostaining images of MSC–NVs-siRNA distribution in lung tissues 4 h after inhalation administration, showing the cellular localization of MSC–NVs in the bronchus and alveolar regions. Scale bar: 100 μm in parenchymal sections. Scale bar: 50 μm in the bronchus and alveolar sections; (F) Percentages of Cy5+ cells in the lungs; (G) Percentages of Cy5+ cells and MFI of MSC–NVs-Cy5-siRNA in different lung cells of asthmatic mice ($n = 6$); Different cell subtypes were marked with corresponding antibodies, including (H) anti-CD45 (immune cells), (I) anti-CD31 (endothelial cells) and (J) anti-EpCAM (epithelial cells). ICs, immune cells; ECs, endothelial cells; and EpiCs, epithelial cells. Data are presented as the means ± SD. Statistical significance was calculated using ordinary two-way ANOVA in (D) or ordinary one-way ANOVA in (G). The *P*-value indicates the statistical difference between the groups, while ns indicates no statistical difference.

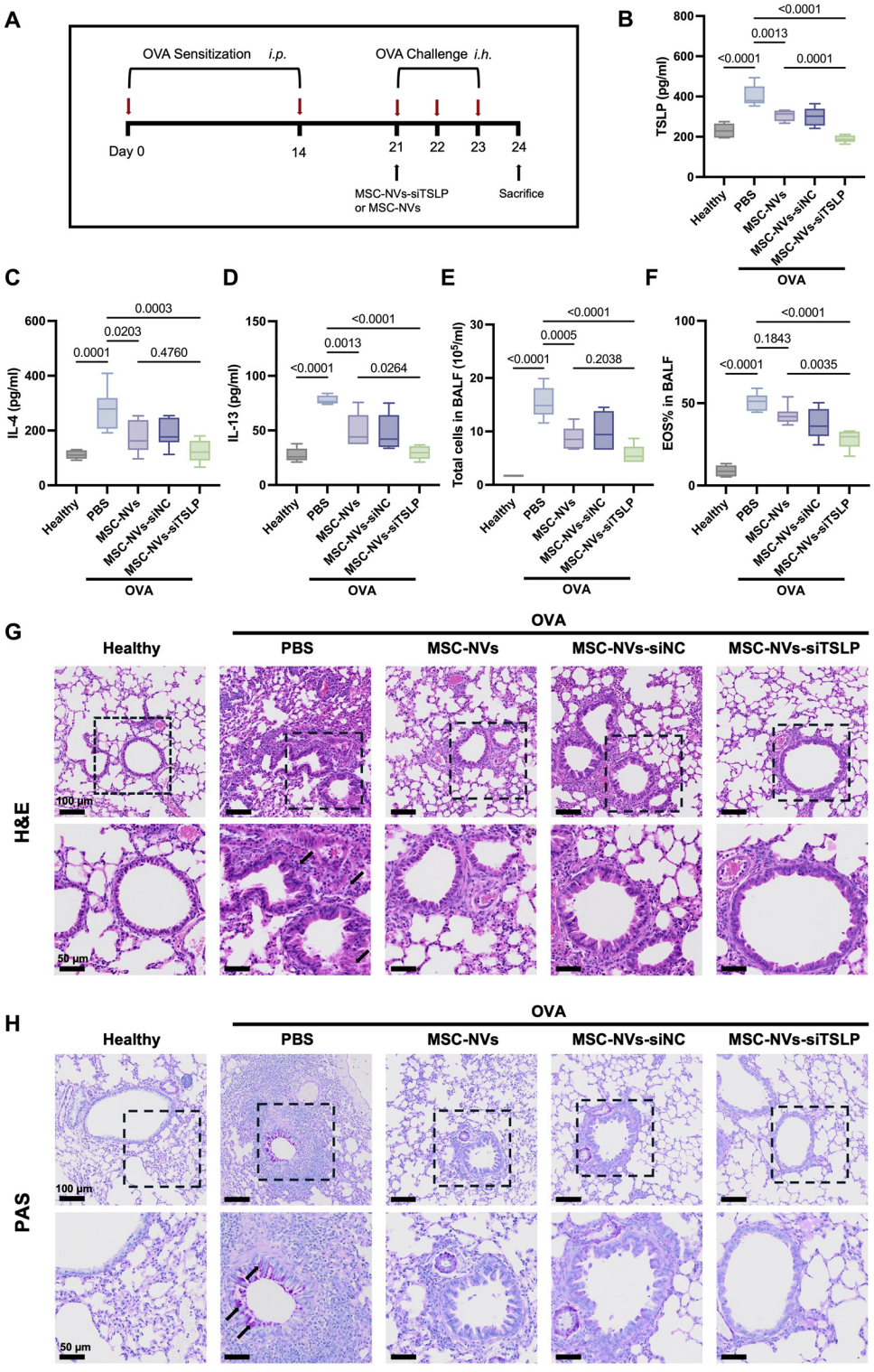


Fig. 5 – *In vivo* therapeutic evaluation of inhalable siRNA-mediated TSLP downregulation in an asthma model. (A) Experimental design of asthma model development and treatment protocol; ELISA quantification of (B) TSLP, (C) IL-4, and (D) IL-13 levels in the BALF ($n = 6$); Total cell counts (E) and the proportion of eosinophils (F) in the BALF ($n = 6$); Images of (G) H&E staining demonstrating inflammatory cell infiltration and (H) PAS staining showing goblet cell hyperplasia after various treatments. Scale bar: 100 μm in the upper panel. Scale bar: 50 μm in the bottom panel. Data are presented as the means ± SD. Statistical significance was calculated using ordinary one-way ANOVA. The *P*-value indicates the statistical difference between the groups.

attenuated TSLP levels, potentially attributable to the immunomodulatory property of these vesicles inherited from inherit their parental MSC [47]. Furthermore, MSC–NVs-siTSLP exhibited a more efficient inhibition of TSLP levels compared to MSC–NVs alone, showing a synergistic therapeutic effect. TSLP is an upstream inflammatory factor in the pathogenesis of asthma, regulating the expression of several Th2 cytokines, such as IL-4 and IL-13 [48]. Results observed in Fig. 5C and 5D were consistent with this notion, wherein the levels of IL-4 and IL-13 across various groups generally aligned with TSLP expression.

Signaling pathways involved in the progression of asthma regulated by TSLP are also reflected in the total number of inflammatory cells and the eosinophil ratio [49]. As presented in Fig. 5E, compared to PBS-treated controls, inhalation of MSC–NVs, MSC–NVs-siNC, or MSC–NVs-siTSLP significantly decreased total inflammatory cell counts, with the greatest reduction observed in the MSC–NVs-siTSLP group. In addition, the proportion of eosinophils showed no significant decrease after the inhalation of MSC–NVs or MSC–NVs-siNC. However, MSC–NVs-siTSLP successfully reduced eosinophil levels (Fig. 5F), indicating that siTSLP-mediated downregulation of TSLP significantly enhanced the therapeutic efficacy of MSC–NVs in asthmatic mice.

In addition, the upregulation of IL-4 and IL-13 further leads to an increased number of goblet cells in airway epithelium, known as goblet cell hyperplasia, which in turn results in excessive mucus secretion and constitutes one of the prominent pathological features of asthma [21]. Therefore, H&E and PAS staining were performed to further evaluate the therapeutic effects of inhalable MSC–NVs-siTSLP in inhibiting the IL-4 and IL-13-induced airway inflammation and goblet cell hyperplasia. As shown in Fig. 5G, there was a notable increase in inflammatory cell infiltration around the bronchi and alveolar regions in the PBS-treated group compared to the healthy group (indicated by the arrows). Similarly, obvious goblet cell hyperplasia was observed in the PBS-treated group, as presented in Fig. 5H (indicated by the arrows). The inhalation of MSC–NVs, MSC–NVs-siNC, or MSC–NVs-siTSLP reduced the infiltration of inflammatory cells and the proliferation of PAS-positive cells. Notably, MSC–NVs-siTSLP most significantly prevented inflammatory cell infiltration and hyperplasia of PAS-positive cells, probably due to their synergistic effect. Collectively, inhalable MSC–NVs endowed an effective delivery of siTSLP through inhalation administration, providing a promising strategy for asthma treatment.

To further validate the therapeutic advantages of MSC–NVs-mediated siRNA delivery in asthma treatment, the *in vivo* therapeutic performances of both inhalation administrated MSC–NVs-siTSLP and MC3-LNP-siTSLP at the same siRNA dose were compared. Considering that TSLP is the direct target of the therapeutic siRNA and a pivotal upstream cytokine driving Th2 inflammation, we assessed the expression levels of both TSLP and its downstream effector IL-4. As shown in Fig. S5, inhalation of MC3-LNP-siTSLP did not significantly reduce the levels of either TSLP or IL-4 compared to the asthma model group. In contrast, treatment with MSC–NVs-siTSLP resulted a substantial decrease in both cytokines, indicating that MSC–NVs-mediated siRNA delivery achieved a more potent anti-inflammatory effect. These results highlight superior therapeutic efficacy of MSC–NVs than their MC3-LNPs-based counterparts for asthma treatment. In addition, no significant loss in body weight was noted (Fig. S6) and no mice were died throughout the treatment processs, indicating the relative saftey of MSC–NVs.

3.6. *Preliminary safety evaluations confirm the relative safety of inhalable MSC–NVs*

Thus far, we have shown the therapeutic potential of MSC–NVs in delivering siTSLP for asthma treatment. We subsequently assessed the potential risks of MSC–NVs as an inhalable delivery platform for siRNA delivery in asthma treatment. The evaluation encompassed both acute (3-d) and subacute (30-d) exposure periods, providing critical insights into the potential biological responses and safety parameters associated with this novel therapeutic approach.

In acute risks, as shown in Fig. 6A, inhalation administration of MSC–NVs and MSC–NVs-siRNA did not increase the expression levels of IL-1β, IL-6 and TNF-α in BALF. Similarly, the total number of inflammatory cells in BALF exhibited no significant differences among all the groups (Fig. 6B). Furthermore, histological evaluation through H&E staining demonstrated that the lungs of PBS-treated mice displayed well-defined alveolar spaces and intact bronchial walls, with no evidence of inflammatory cell infiltration. Similarly, the histological characteristics of the MSC–NVs and MSC–NVs-siRNA treatment groups closely resembled those of the PBS group, showing no detectable inflammatory lesions in the airways or alveolar regions (Fig. 6C). Moreover, no significant neutrophil or macrophage infiltration was observed in the lung tissues of the MSC–NVs and MSC–NVs-siRNA treatment groups, as shown by immunohistochemical staining in Fig. 6D and 6E. These results indicated that the inhalation administration of MSC–NVs did not induce severe side effects on the respiratory system. As presented in Fig. 6F and 6G, neither the number of leukocytes nor the ratios of neutrophils in the blood samples were affected by the inhalation administration of MSC–NVs and MSC–NVs-siRNA in healthy mice, suggesting that MSC–NVs did not cause severe systemic inflammatory responses. Similarly, no significant changes were observed in red blood cell and platelet counts in the blood, confirming no notable side effects on the erythrocyte or platelet systems (Fig. 6H and 6I). In subacute safety assessments, comprehensive evaluations performed at the 1-month time point following both single-dose and repeated-dose inhalation administration of MSC–NVs and MSC–NVs-siRNA. No obvious alterations were noted in inflammatory cytokine expressions, pulmonary histopathological characteristics, or peripheral blood parameters. These examinations collectively suggest that prolonged exposure time or repeated administration of MSC–NVs and their siRNA complexes does not elicit substantial pulmonary toxicity or induce adverse immune responses, thereby supporting the long-term safety profile of this therapeutic approach (Fig. S7).

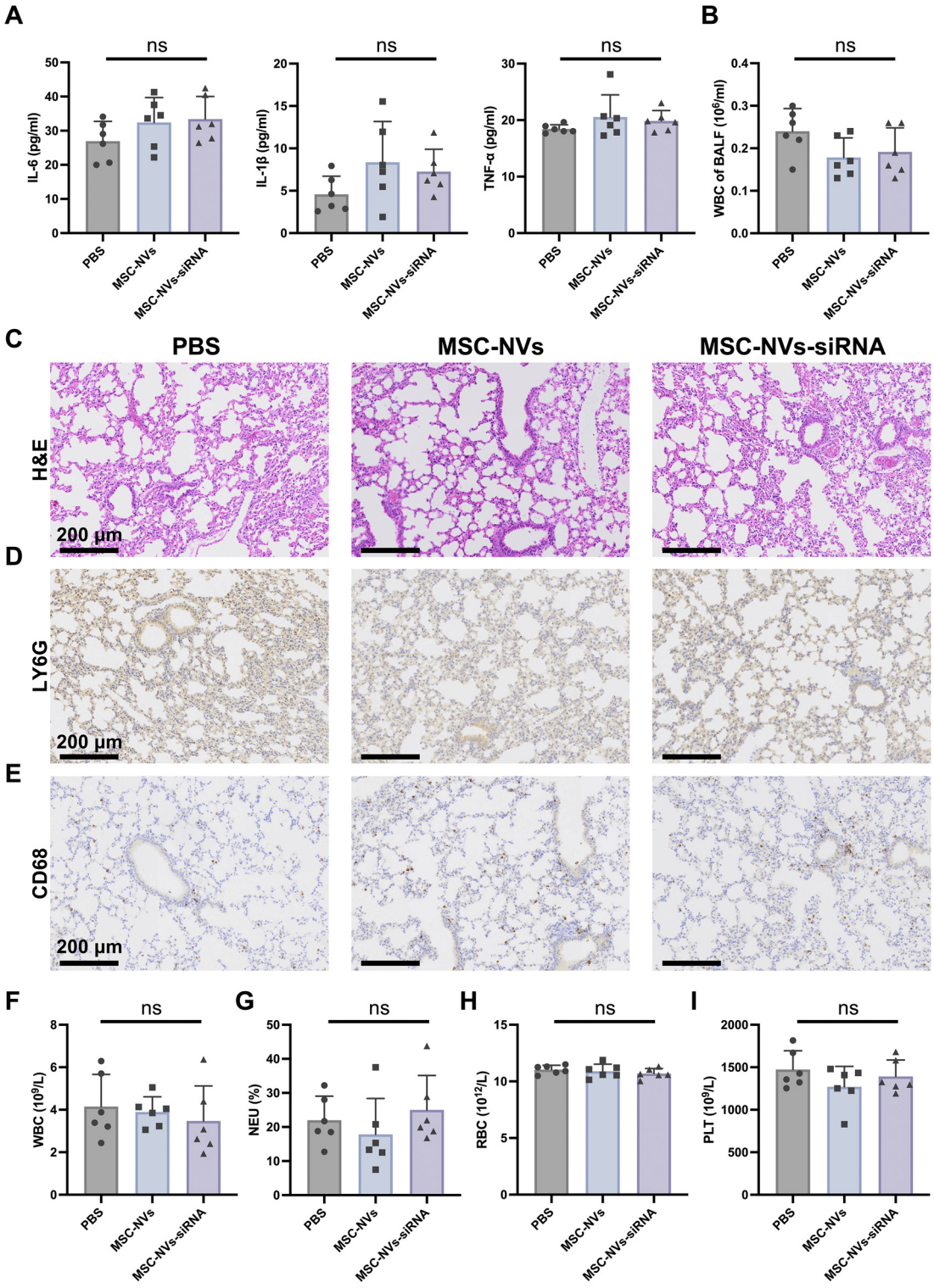


Fig. 6 – Preliminary safety evaluation of single-dose inhalation administration of MSC–NVs and MSC–NVs-siRNA. (A) Concentrations of IL-6, IL-1β, and TNF-α in collected BALF after the indicated treatments (n = 6); (B) Cell density of leukocytes in collected BALF after the indicated treatments (n = 6); (C) H&E staining images demonstrating inflammatory cell infiltration. Scale bar: 200 μm; (D) Immunoenzymatic staining images showing neutrophil infiltration. Scale bar: 200 μm; (E) Immunoenzymatic staining images demonstrating macrophage infiltration. Scale bar: 200 μm; (F) Leukocyte counts in the blood (n = 6); (G) Neutrophils ratios among total leukocytes in the blood (n = 6); (H) Red blood cell counts in the blood (n = 6); (I) Platelet counts in the blood (n = 6). Data are presented as the means ± SD. Statistical significance was calculated using ordinary one-way ANOVA. ns indicates no statistical difference between the groups.

4. Conclusions

In conclusion, the present study proposed a promising strategy for effective and targeted siRNA delivery using inhalable nanovesicles artificially prepared from MSCs. By carefully modifying the extrusion process, MSC–NVs with optimal properties and high yield were successfully acquired in this study. These MSC–NVs further demonstrated the potential as an inhalable vehicle for siRNA delivery, significantly downregulating the upstream cytokine TSLP in asthmatic inflammatory cascades. Consequently, MSC–NVs loaded with siTSLP successfully inhibited the initiation of TSLP-driven inflammatory responses and goblet cell hyperplasia, thereby relieving the asthma symptom. It is also important to acknowledge that the current study utilized an OVA-induced asthma model [50,51], which primarily representing a Th2-dominant phenotype and may not fully capture human asthma heterogeneity, such as neutrophilic or steroid-resistant subtypes. Nevertheless, MSC–NVs possess intrinsic immunomodulatory capability from their parent MSCs, including the regulation of T cell differentiation and macrophage polarization, which allow them to suppress both eosinophilic and neutrophilic inflammation [52]. Additionally, MSC–NVs can serve as a versatile delivery platform for siRNAs targeting inflammatory mediators associated with non-Th2 asthma [53]. These characteristics suggest that MSC–NVs could potentially be applied across diverse asthma phenotypes, extending beyond the present Th2-dominant asthma model. Considering MSC–NVs' easy preparation, high yield, and inherent immunomodulatory capability, we believe they hold significant promise as a delivery platform for inhalable nucleic acid drugs. Moreover, the inhalable MSC–NVs represent a promising and efficient pulmonary delivery strategy for the treatment of diverse pulmonary diseases. Nevertheless, it is still necessary to recognize a limitation related to their cellular targeting specificity. Although both the inhalation administration route and the presence of membrane proteins such as CD9 and CD63 on MSC–NVs facilitate their efficient uptake by AECs, MSC–NVs lack precise specificity for inflamed cells. Future studies could focus on the functionalization of MSC–NVs with targeting ligands or surface modifications designed to enhance selective uptake by activated AECs, thereby further improving their treatment precision and therapeutic efficiency. Furthermore, several practical hurdles remain to be addressed before MSC–NVs can advance toward clinical translation. Requirements of their large-scale production necessitates the development of robust bioreactor-based culture systems for efficient MSCs expansion, coupled with standardized extrusion and purification protocols. However, achieving consistent batch-to-batch reproducibility while maintaining cost-effectiveness in manufacturing remains a significant hurdle. Moreover, storage stability also poses another major concern. Current nanovesicles storage approaches, primarily relying on deep freezing [54], face challenges such as aggregation during freeze-thaw cycles, loss of membrane integrity and cargo leakage due to ice crystal formation, reduced biological activity over time, as well as logistical burdens of maintaining ultra-low temperatures [55–57]. Alternative preservation strategies, including lyophilization and the optimization of cryoprotectant formulations, are under active investigation to enhance vesicle integrity and extend shelf life [58]. Furthermore, in the context of nebulization, particular attention must be paid to three key characteristics: vesicle structural stability, dose uniformity, and aerosol particle size [59]. The selection of nebulizer type and operating parameters should be carefully optimized based on the physicochemical properties of the formulation to maximize delivery efficiency and therapeutic outcomes.

Conflicts of interest

The authors declare that there is no conflicts of interest.

CRediT authorship contribution statement

Shihan Chen: Writing – original draft, Methodology, Investigation, Formal analysis, Data curation. **Ruyi Lin:** Methodology, Investigation, Data curation. **Yuhuan Kong:** Methodology, Investigation. **Hao Sun:** Methodology, Investigation. **Jiawen Wang:** Methodology, Investigation. **Jinsong Zhang:** Methodology, Investigation. **Yanshuang Huang:** Investigation. **Honghui Wu:** Writing – review & editing. **Donghang Xu:** Resources, Funding acquisition. **Jianqing Gao:** Writing – review & editing, Supervision, Resources, Project administration, Funding acquisition. **Tianyuan Zhang:** Writing – review & editing, Validation, Supervision, Funding acquisition, Data curation, Conceptualization.

Acknowledgments

This work was supported by National Natural Science Foundation of China (U22A20383), Natural Science Foundation of Zhejiang Province (LY24H300001), Fundamental Research Funds for the Central Universities (226-2022-00125), Zhejiang Province Postdoctoral Research Excellence Funding Project (ZJ2023151), and Pharmacy 80 Basic Research Funding in College of Pharmaceutical Sciences, Zhejiang University Education Foundation. We would like to thank Prof. Chao Zhang from College of Medicine, Zhejiang University for her help and advice about asthma mice model construction. We would also like to thank Ms. Chenyu Yang in the Center of Cryo-Electron Microscopy (CCEM), Zhejiang University for her technical assistance on Transmission Electron Microscopy.

Supplementary materials

Supplementary material associated with this article can be found, in the online version, at doi:10.1016/j.ajps.2026.101122. The figures and tables with "S" before the serial number are included in the Supplementary data.

References

[1] Papi A, Brightling C, Pedersen SE, Reddel HK. Asthma. Lancet 2018;391(10122):783–800.

[2] GBD 2017 Disease and Injury Incidence and Prevalence Collaborators. Global, regional, and national incidence, prevalence, and years lived with disability for 354 diseases and injuries for 195 countries and territories, 1990-2017: a systematic analysis for the Global Burden of Disease Study 2017. Lancet 2018;392(10159):1789–858.

[3] Lommatzsch M, Brusselle GG, Levy ML, Canonica GW, Pavord ID, Schatz M, et al. A2BCD: a concise guide for asthma management. Lancet Respir Med 2023;11(6):573–6.

[4] Bleecker ER, Menzies-Gow AN, Price DB, Bourdin A, Sweet S, Martin AL, et al. Systematic literature review of systemic corticosteroid use for asthma management. Am J Respir Crit Care Med 2020;201(3):276–93.

[5] Varricchi G, Brightling CE, Grainge C, Lambrecht BN, Chanez P. Airway remodelling in asthma and the epithelium: on the edge of a new era. Eur Respir J 2024;63(4):2301619.

[6] Lu H, Liu X, Zhang M, Bera H, Xu W, Jiang H, et al. Pulmonary fibroblast-specific delivery of siRNA exploiting exosomes-based nanoscaffolds for IPF treatment. Asian J Pharm Sci 2024;19(4):100929.

[7] You H, Zhang S, Zhang Y, Chen Q, Wu Y, Zhou Z, et al. Engineered bacterial outer membrane vesicles-based doxorubicin and CD47-siRNA co-delivery nanoplatform overcomes immune resistance to potentiate the immunotherapy of glioblastoma. Adv Mater 2025;37(15):e2418053.

[8] Keil TWM, Baldassi D, Merkel OM. T-cell targeted pulmonary siRNA delivery for the treatment of asthma. Wiley Interdiscip Rev Nanomed Nanobiotechnol 2020;12(5):e1634.

[9] Russell RJ, Boulet LP, Brightling CE, Pavord ID, Porsbjerg C, Dorscheid D, et al. The airway epithelium: an orchestrator of inflammation, a key structural barrier and a therapeutic target in severe asthma. Eur Respir J 2024;63(4):2301397.

[10] Gauvreau GM, Sehmi R, Ambrose CS, Griffiths JM. Thymic stromal lymphopoietin: its role and potential as a therapeutic target in asthma. Expert Opin Ther Targets 2020;24(8):777–92.

[11] Moazzam M, Zhang M, Hussain A, Yu X, Huang J, Huang Y. The landscape of nanoparticle-based siRNA delivery and therapeutic development. Mol Ther 2024;32(2):284–312.

[12] Witwer KW, Wolfram J. Extracellular vesicles versus synthetic nanoparticles for drug delivery. Nat Rev Mater 2021;6(2):103–6.

[13] Khalil IA, Yamada Y, Harashima H. Optimization of siRNA delivery to target sites: issues and future directions. Expert Opin Drug Deliv 2018;15(11):1053–65.

[14] Bai X, Chen Q, Li F, Teng Y, Tang M, Huang J, et al. Optimized inhaled LNP formulation for enhanced treatment of idiopathic pulmonary fibrosis via mRNA-mediated antibody therapy. Nat Commun 2024;15(1):6844.

[15] Deng X, Yang Y, Gan L, Duan X, Wang X, Zhang J, et al. Engineering lipid nanoparticles to enhance intracellular delivery of transforming growth factor-beta siRNA (siTGF-β1) via inhalation for improving pulmonary fibrosis post-bleomycin challenge. Pharmaceutics 2025;17(2):157.

[16] Patel AK, Kaczmarek JC, Bose S, Kauffman KJ, Mir F, Heartlein MW, et al. Inhaled nanoformulated mRNA polyplexes for protein production in lung epithelium. Adv Mater 2019;31(8):e1805116.

[17] Sun H, Zhang T, Gao J. Extracellular vesicles derived from mesenchymal stem cells: a potential biodrug for acute respiratory distress syndrome treatment. BioDrugs 2022;36(6):701–15.

[18] Jiang XC, Wu HH, Zhang T, Dong YF, Li YS, Huang T, et al. Biological nano agent produced by hypoxic preconditioning stem cell for stroke treatment. Nano Res 2023;16(5):7413–21.

[19] Han Y, Zhu Y, Youngblood HA, Almuntashiri S, Jones TW, Wang X, et al. Nebulization of extracellular vesicles: a promising small RNA delivery approach for lung diseases. J Control Release 2022;352:556–69.

[20] Fu Z, Zhang X, Zhou X, Ur-Rehman U, Yu M, Liang H, et al. *In vivo* self-assembled small RNAs as a new generation of RNAi therapeutics. Cell Res 2021;31(6):631–48.

[21] Liu M, Hu S, Yan N, Popowski KD, Cheng K. Inhalable extracellular vesicle delivery of IL-12 mRNA to treat lung cancer and promote systemic immunity. Nat Nanotechnol 2024;19(4):565–75.

[22] Zhu D, Liu S, Huang K, Li J, Mei X, Li Z, et al. Intrapericardial long non-coding RNA-Tcf21 antisense RNA inducing demethylation administration promotes cardiac repair. Eur Heart J 2023;44(19):1748–60.

[23] Ding L, Tang S, Wyatt TA, Knoell DL, Oupický D. Pulmonary siRNA delivery for lung disease: review of recent progress and challenges. J Control Release 2021;330:977–91.

[24] Sun D, Mou S, Chen L, Yang J, Wang R, Zhong A, et al. High yield engineered nanovesicles from ADSC with enriched miR-21-5p promote angiogenesis in adipose tissue regeneration. Biomater Res 2022;26(1):83.

[25] Jiang XC, Zhang T, Gao JQ. The *in vivo* fate and targeting engineering of crossover vesicle-based gene delivery system. Advanced Drug Delivery Reviews 2022;187:114324.

[26] Wang X, Hu S, Li J, Zhu D, Wang Z, Cores J, et al. Extruded mesenchymal stem cell nanovesicles are equally potent to natural extracellular vesicles in cardiac repair. ACS Appl Mater Interfaces 2021;13(47):55767–79.

[27] Wang X, Hu S, Zhu D, Li J, Cheng K, Liu G. Comparison of extruded cell nanovesicles and exosomes in their molecular cargos and regenerative potentials. Nano Res 2023;16(5):7248–59.

[28] Arya SB, Collie SP, Parent CA. The ins-and-outs of exosome biogenesis, secretion, and internalization. Trends Cell Biol 2024;34(2):90–108.

[29] Hirosawa KM, Sato Y, Kasai RS, Yamaguchi E, Komura N, Ando H, et al. Uptake of small extracellular vesicles by recipient cells is facilitated by paracrine adhesion signaling. Nat Commun 2025;16(1):2419.

[30] Kou M, Huang L, Yang J, Chiang Z, Chen S, Liu J, et al. Mesenchymal stem cell-derived extracellular vesicles for immunomodulation and regeneration: a next generation therapeutic tool? Cell Death Dis 2022;13(7):580.

[31] Chen S, Gao J, Zhang T. From mesenchymal stem cells to their extracellular vesicles: progress and prospects for asthma therapy. Asian J Pharm Sci 2024;19(4):100942.

[32] Mu J, Li L, Wu J, Huang T, Zhang Y, Cao J, et al. Hypoxia-stimulated mesenchymal stem cell-derived exosomes loaded by adhesive hydrogel for effective angiogenic treatment of spinal cord injury. Biomater Sci 2022;10(7):1803–11.

[33] Li L, Zhang Y, Mu J, Chen J, Zhang C, Cao H, et al. Transplantation of human mesenchymal stem-cell-derived exosomes immobilized in an adhesive hydrogel for effective treatment of spinal cord Injury. Nano Lett 2020;20(6):4298–305.

[34] Kim HY, Bhang SH. Stem cell-engineered nanovesicles exert proangiogenic and neuroprotective effects. Materials (Basel) 2021;14(5):1078.

[35] Bandeira E, Jang SC, Lässer C, Johansson K, Rådinger M, Park KS. Effects of mesenchymal stem cell-derived nanovesicles in experimental allergic airway inflammation. Respir Res 2023;24(1):3.

[36] Li Z, Cheng Q, Lin L, Fu X, Wang Y. Plasma membrane-derived biomimetic apoptotic nanovesicles targeting inflammation and cartilage degeneration for osteoarthritis. Small Methods 2025;9(1):e2400660.
[37] Zelepukin IV, Shevchenko KG, Deyev SM. Rediscovery of mononuclear phagocyte system blockade for nanoparticle drug delivery. Nat Commun 2024;15(1):4366.
[38] García-Fernández A, Sancenón F, Martínez-Máñez R. Mesoporous silica nanoparticles for pulmonary drug delivery. Adv Drug Deliv Rev 2021;177:113953.
[39] Muskan M, Abeysinghe P, Cecchin R, Branscome H, Morris KV, Kashanchi F. Therapeutic potential of RNA-enriched extracellular vesicles: the next generation in RNA delivery via biogenic nanoparticles. Mol Ther 2024;32(9):2939–49.
[40] Bai X, Zhao G, Chen Q, Li Z, Gao M, Ho W, et al. Inhaled siRNA nanoparticles targeting IL11 inhibit lung fibrosis and improve pulmonary function post-bleomycin challenge. Sci Adv 2022;8(25):eabn7162.
[41] Lai JJ, Chau ZL, Chen SY, Hill JJ, Korpany KV, Liang NW, et al. Exosome processing and characterization approaches for research and technology development. Adv Sci (Weinh) 2022;9(15):e2103222.
[42] Dominici M, Le Blanc K, Mueller I, Slaper-Cortenbach I, Marini F, Krause D, et al. Minimal criteria for defining multipotent mesenchymal stromal cells. The International Society for Cellular Therapy position statement. Cytotherapy 2006;8(4):315–17.
[43] Miller RL, Grayson MH, Strothman K. Advances in asthma: new understandings of asthma's natural history, risk factors, underlying mechanisms, and clinical management. J Allergy Clin Immunol 2021;148(6):1430–41.
[44] Liu Q, Guan J, Qin L, Zhang X, Mao S. Physicochemical properties affecting the fate of nanoparticles in pulmonary drug delivery. Drug Discov Today 2020;25(1):150–9.
[45] He Y, Liang Y, Han R, Lu WL, Mak JCW, Zheng Y. Rational particle design to overcome pulmonary barriers for obstructive lung diseases therapy. J Control Release 2019;314:48–61.
[46] Liu Q, Guan J, Song R, Zhang X, Mao S. Physicochemical properties of nanoparticles affecting their fate and the physiological function of pulmonary surfactants. Acta Biomater 2022;140:76–87.
[47] Mirershadi F, Ahmadi M, Rezabakhsh A, Rajabi H, Rahbarghazi R, Keyhanmanesh R. Unraveling the therapeutic effects of mesenchymal stem cells in asthma. Stem Cell Res Ther 2020;11(1):400.
[48] Hong H, Liao S, Chen F, Yang Q, Wang DY. Role of IL-25, IL-33, and TSLP in triggering united airway diseases toward type 2 inflammation. Allergy 2020;75(11):2794–804.
[49] Siddiqui S, Bachert C, Bjermer L, Buchheit KM, Castro M, Qin Y, et al. Eosinophils and tissue remodeling: relevance to airway disease. J Allergy Clin Immunol 2023;152(4):841–57.
[50] Du X, Li F, Zhang C, Li N, Huang H, Shao Z, et al. Eosinophil-derived chemokine (hCCL15/23, mCCL6) interacts with CCR1 to promote eosinophilic airway inflammation. Signal Transduct Target Ther 2021;6(1):91.
[51] Chen S, Chen G, Xu F, Sun B, Chen X, Hu W, et al. Treatment of allergic eosinophilic asthma through engineered IL-5-anchored chimeric antigen receptor T cells. Cell Discov 2022;8(1):80.
[52] Huang S, Li Y, Zeng J, Chang N, Cheng Y, Zhen X, et al. Mesenchymal Stem/stromal cells in asthma therapy: mechanisms and strategies for enhancement. Cell Transplant 2023;32:9636897231180128.
[53] Kumar S, Corkran M, Cheema Y, Scull MA, Duncan GA. AAV-mediated MUC5AC siRNA delivery to prevent mucociliary dysfunction in asthma. Gene Ther 2025;32(5):508–16.
[54] Ahmadian S, Jafari N, Tamadon A, Ghaffarzadeh A, Rahbarghazi R, Mahdipour M. Different storage and freezing protocols for extracellular vesicles: a systematic review. Stem Cell Res Ther 2024;15(1):453.
[55] Rezabakhsh A, Sokullu E, Rahbarghazi R. Applications, challenges and prospects of mesenchymal stem cell exosomes in regenerative medicine. Stem Cell Res Ther 2021;12(1):521.
[56] Yuan F, Li YM, Wang Z. Preserving extracellular vesicles for biomedical applications: consideration of storage stability before and after isolation. Drug Deliv 2021;28(1):1501–9.
[57] Levy D, Jeyaram A, Born LJ, Chang KH, Abadchi SN, Hsu ATW, et al. Impact of storage conditions and duration on function of native and cargo-loaded mesenchymal stromal cell extracellular vesicles. Cytotherapy 2023;25(5):502–9.
[58] Susa F, Limongi T, Borgione F, Peiretti S, Vallino M, Cauda V, et al. Comparative studies of different preservation methods and relative freeze-drying formulations for extracellular vesicle pharmaceutical applications. ACS Biomater Sci Eng 2023;9(10):5871–85.
[59] Mišík O, Kejíková J, Cejpek O, Malý M, Jugl A, Bělka M, et al. Nebulization and *in vitro* upper airway deposition of liposomal carrier systems. Mol Pharm 2024;21(4):1848–60.